

FreeGen: Feed-Forward Reconstruction–Generation Co-Training for Free-Viewpoint Driving Scene Synthesis

Shijie Chen Peixi Peng 

School of Electronic and Computer Engineering, Peking University

{2501111941@stu., p xpeng}@pku.edu.cn

Abstract

Closed-loop simulation and scalable pre-training for autonomous driving require synthesizing free-viewpoint driving scenes. However, existing datasets and generative pipelines rarely provide consistent off-trajectory observations, limiting large-scale evaluation and training. While recent generative models demonstrate strong visual realism, they struggle to jointly achieve interpolation consistency and extrapolation realism without per-scene optimization. To address this, we propose FreeGen, a feed-forward reconstruction-generation co-training framework for free-viewpoint driving scene synthesis. The reconstruction model provides stable geometric representations to ensure interpolation consistency, while the generation model performs geometry-aware enhancement to improve realism at unseen viewpoints. Through co-training, generative priors are distilled into the reconstruction model to improve off-trajectory rendering, and the refined geometry in turn offers stronger structural guidance for generation. Experiments demonstrate that FreeGen achieves state-of-the-art performance for free-viewpoint driving scene synthesis.

1. Introduction

Robust autonomous driving systems require virtual environments for scalable pretraining and closed-loop policy evaluation [20, 21, 23]. However, existing real [4, 14, 34] and synthetic driving data [11, 12, 37] are predominantly collected along a single trajectory, providing limited coverage of the diverse trajectories induced by different actions. The scarcity of off-trajectory observations hinders high-fidelity and consistent rendering at free-viewpoints [6, 8, 40, 41]. The key challenge lies in achieving high-quality free-viewpoint driving scene synthesis across different trajectories using only single-trajectory observations.

To this end, a practical solution should satisfy three requirements: (1) **Interpolation Consistency**. Preserve geometric consistency with the observed views in their over-

Table 1. **Comparison of different methods.** We consider interpolation consistency (Interp. Consistency), extrapolation realism (Extrap. Realism), and whether supports feed-forward inference.

Method	Interp. Consistency	Extrap. Realism	Feed-forward
3DGS [24]	✓	✗	✗
PVG [6]	✓	✗	✗
UniSim [42]	✓	✗	✗
EmerNeRF [41]	✓	✗	✗
StreetGaussian [40]	✓	✗	✗
OmniRe [8]	✓	✗	✗
DriveDreamer4D [45]	✓	✓	✗
ReconDreamer [28]	✓	✓	✗
DriveX [43]	✓	✓	✗
FreeSim [10]	✓	✓	✗
DrivingForward [35]	✓	✗	✓
Omni-Scene [39]	✓	✗	✓
FreeVS [36]	✗	✓	✓
DiST-4D [15]	✗	✓	✓
FreeGen (Ours)	✓	✓	✓

lapping regions. (2) **Extrapolation Realism**. Generate visually plausible content that matches the underlying distribution at unseen viewpoints. (3) **Feed-forward**. Synthesize the scene in a single forward pass instead of iterative refinement, enabling scalability with data-driven advances (e.g., scaling laws) for large-scale driving scene generation.

We compare current methods in Tab. 1. Traditional reconstruction-based methods [6, 8, 40, 41] excel at enforcing interpolation consistency but are fundamentally limited to interpolating within sparse observations, making it difficult to render free-viewpoint views. They typically require per-scene optimization, leading to prohibitive computational costs that hinder large-scale scene synthesis. Recent feed-forward reconstruction approaches [35, 39] enable efficient scene reconstruction in a single pass but still struggle to produce realistic details at extrapolated views. With the rapid progress of generative models, data-driven methods trained on large-scale videos [3, 13, 37] show strong potential for generating realistic views from sparse inputs, yet they generally lack fine-grained control over camera trajectories. Hybrid methods that combine generative mod-



Figure 1. **Complementary strengths of reconstruction and generation methods.** Reconstruction maintains geometry but lacks realistic textures, generation improves realism but often distorts geometry. Our method combines both, achieving consistent and realistic results.

els with reconstruction-based pipelines [10, 28, 43, 45] enhance visual detail while preserving interpolation consistency, but often require hours to days of per-scene training, undermining their practicality for feed-forward inference.

Recent methods leverage free-viewpoint rendered views to guide generative refinement for high-quality feed-forward scene synthesis [15, 36]. However, LiDAR conditions [36] are sparse and expensive, making it difficult to cover distant buildings and sky, while image warping conditions [15] often introduce structural misalignment (e.g., missing utility poles and distorted pedestrians in Fig. 1). Moreover, these conditions are non-learnable, limiting their ability to benefit from large-scale image data.

We observe that reconstruction and generation approaches offer complementary strengths for free-viewpoint driving scene synthesis. As shown in Fig. 1, reconstruction models excel at preserving geometric and interpolation consistency but are limited in fine details at unseen viewpoints. In contrast, generation models can produce visually realistic results from sparse observations, yet often introduce structural distortions with respect to the input views. This complementarity motivates us to unify these two paradigms in a single feed-forward framework that preserves geometric faithfulness while leveraging generative realism.

To address the aforementioned challenges, we propose **FreeGen**, a feed-forward reconstruction-generation framework for free-viewpoint driving scene synthesis. We first employs a feed-forward 3D Gaussian Splatting (3DGS) model to efficiently reconstruct scene from sparse input images without per-scene optimization. Then We renders views along free-viewpoint trajectories to enforce interpolation consistency with the observed inputs. These rendered views are then used as geometric guidance for a generative refinement model, enabling realistic extrapolation at unseen viewpoints. Moreover, FreeGen does not require additional expensive annotations such as LiDAR or bounding boxes, relying solely on a single trajectory image data, which make it practical for large-scale driving scene synthesis.

Our method builds upon recent advances in feed-forward 3DGS [39] and video diffusion models [3]. To fully exploit their complementary strengths, we introduce two key de-

signs in FreeGen. The reconstruction branch already produces structurally complete renderings with minimal visible holes, but due to limited supervision from a single trajectory, a naive generative module cannot reliably localize subtle artifacts. To address this, we **construct geometry conditions** based on the 3DGS rendering mechanism and incorporate a **geometry-aware diffusion refinement** module to guide appearance refinement. In addition, we propose a **co-training** strategy that samples viewpoints off the input trajectory and forms a closed loop between reconstruction and generation. The generative priors distilled during refinement are fed back into the reconstruction model to improve free-viewpoint rendering quality, while the reconstruction model provides geometric guidance to construct closed-loop supervision for the generative module.

Our contributions are summarized as follows:

- We introduce FreeGen, a feed-forward reconstruction-generation co-training framework for free-viewpoint driving scene synthesis, which achieves both interpolation consistency and extrapolation realism without per-scene optimization or additional expensive annotations.
- We propose a geometry-aware diffusion refinement module to achieve high-quality refinement on reconstructed views. To further improve both reconstruction and generation performance at off-trajectory viewpoints, we introduce a closed-loop co-training strategy.
- Extensive experiments demonstrate that FreeGen outperforms existing approaches in free-viewpoint driving scene synthesis.

2. Related Work

Driving Scene Synthesis with Reconstruction. Early methods employed Neural Radiance Fields (NeRF) [1, 2, 26, 27] to model scenes with MLPs and enable free-viewpoint image synthesis, but they suffer from slow training and rendering. The advent of 3DGS [24] has significantly advanced this paradigm. By leveraging explicit point-based representations and rasterization-based rendering, 3DGS achieves much faster training and inference. Recent works [39, 40] extend 3DGS to driving scenarios. However, they mainly focus on viewpoints along

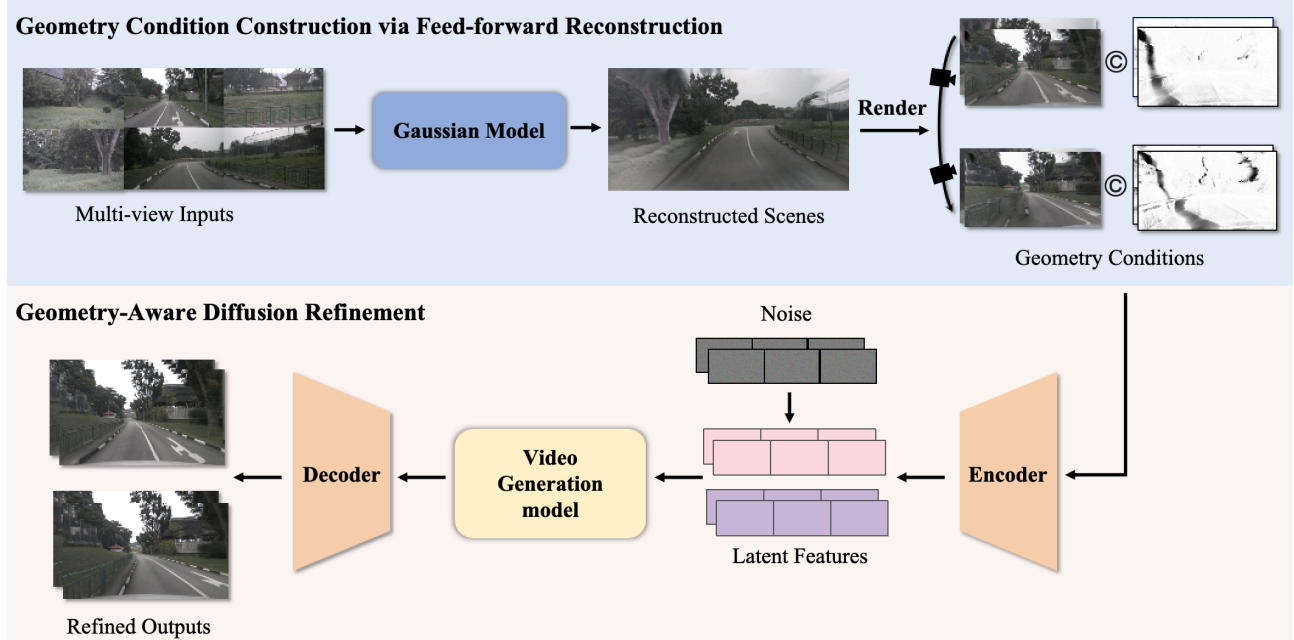


Figure 2. **Overview of the proposed FreeGen.** The reconstruction model encodes multi-view inputs into Gaussian features and decodes them into 3DGS representations. The rendered views and corresponding opacity maps are then used to guide the geometry-aware diffusion model, which performs fine-grained refinement. For clarity, depth maps are omitted from the illustration.

the training trajectory and often rely on per-scene optimization, which limits their scalability for large-scale driving scene synthesis. In addition, most of these methods [39, 40] require extra expensive annotations, such as point clouds or bounding boxes. Recent feed-forward 3DGS [5, 7, 35] methods achieve efficient scene reconstruction by predicting 3D Gaussians in a single forward pass. Omni-Scene [39] further combines pixel and voxel branches to improve render quality at viewpoints beyond the input views, leading to higher-quality driving scene reconstruction. However, these approaches still primarily target viewpoints along or near the training trajectory.

Driving Scene Synthesis with Diffusion Prior. Thanks to the rapid development of diffusion-based generative methods [9, 16–18, 30, 33], image generation for driving scenes has made notable progress in recent years [11, 13, 37]. Many works apply diffusion models to free-viewpoint image synthesis in driving environments [3]. Some approaches use diffusion models to refine free-viewpoint rendered views and iteratively optimize the scene representation. DriveDreamer4D [45] employs video diffusion models conditioned on initial recorded frames to synthesize free-viewpoint sequences and optimize dynamic scene representations, but it struggles to precisely control generated content and often suffers from structural misalignment. ReconDreamer [45] trains a video diffusion model on degraded renderings obtained during Gaussian Splatting training to repair free-viewpoint results. DriveX [43] formulates

an inverse problem, using diffusion models to refine free-viewpoint renderings before iteratively updating the scene representation. However, these methods require per-scene optimization during both training and inference, often taking hours to days for a single scene, which makes them difficult to scale to large-scale applications. Other approaches avoid explicitly constructing full 3D scene representations and instead rely on LiDAR or image warping as free-viewpoint rendering proxies. FreeVS [36] guides diffusion-based generation by aggregating multi-frame LiDAR projections, enabling efficient training and feed-forward inference. However, LiDAR inputs are often costly and spatially sparse, especially for distant objects and sky regions, which leads to incomplete guidance. DiST-4D [15] adopts image warping to project observed views to free-viewpoints for diffusion-based generation, but such warping is prone to structural misalignment, making it difficult to maintain consistency between the results and the observations.

3. Methodology

Our key idea is to leverage the complementary strengths of reconstruction and generation to enhance both interpolation consistency and extrapolation realism in free-viewpoint scene synthesis. To achieve this, we first reconstruct the scene from multi-view inputs using a feed-forward reconstruction model, following [39]. Then we perform free-viewpoint rendering along given camera trajectories to obtain rendered views and corresponding geometry conditions

(Sec. 3.1). Next, the rendered results are used to guide a diffusion refinement model (Sec. 3.2). The overall framework of our method is illustrated in Fig. 2. Furthermore, we jointly train the reconstruction and generation models to improve overall performance (Sec. 3.3), as shown in Fig. 3.

3.1. Geometry Condition Construction via Feed-forward Reconstruction

An appropriate scene representation should support both efficient reconstruction and fast rendering. Recent feed-forward 3DGS methods [5, 7, 35, 39] make this possible by reconstructing large-scale driving scenes from multi-view images within seconds, achieving real-time rendering and learning rich scene priors from large-scale data. Motivated by this, we adopt a feed-forward 3DGS-based reconstruction network in FreeGen, following [39].

Given sparse N -view inputs $\{I_i\}_{i=1}^N$ with corresponding camera parameters $\{P_i\}_{i=1}^N$, we first predict depth maps $\{D_i\}_{i=1}^N$ using an off-the-shelf depth estimation model [19] to assist scene reconstruction. We then use a Gaussian encoder to extract Gaussian features. Specifically, we apply a multi-view U-Net style pixel encoder [5, 7, 35, 39] to extract pixel-aligned high-resolution feature maps $\{\mathcal{F}_i^{\text{pixel}}\}_{i=1}^N$. Then we fuse multi-view features into a triplane representation via a Triplane Transformer [22] with deformable attention [25]. Finally, Gaussian decoders transform both pixel and voxel features into a set of K 3D Gaussians [24] $\{G_i = (\delta_i, \alpha_i, s_i, q_i, c_i)\}_{i=1}^K$, where δ_i , α_i , s_i , q_i , and c_i denote the position, opacity, scale, orientation, and color of each Gaussian. We then render the color image I_{geo} , opacity map A_{geo} , and depth map D_{geo} via tile-based rasterization [24]. The color image is computed as follows:

$$I_{\text{geo}} = \sum_{i=1}^K c_i \alpha'_i \prod_{j=1}^{i-1} (1 - \alpha'_j), \quad (1)$$

where α'_i is the screen-space opacity contribution of the i -th Gaussian determined as 3DGS [24]. The opacity map A_{geo} and depth map D_{geo} are obtained similar to the color image. Then we define the geometry conditions C_{geo} as follows:

$$C_{\text{geo}} = [I_{\text{geo}}, D_{\text{geo}}, A_{\text{geo}}]. \quad (2)$$

In FreeGen, the geometry conditions serve as the geometric condition for the diffusion-based generation model, enabling geometry-aware refinement. The color image provides structural and appearance information, the depth map enhances geometric consistency [15], and the opacity map reflects the reliability of the color image, where higher opacity usually corresponds to more reliable renderings.

The training phase of the reconstruction model includes two stages. In the first stage, we follow [39] and train the model on the original single trajectory sequences, forming cross-timestamp pairs to establish reconstruction capability

of the model. In the second training stage, we randomly render views at off-trajectory viewpoints and refine them with the generation model to obtain pseudo-labels. These pseudo-labels then supervise the reconstruction model to improve free-viewpoint rendering. Details are provided in Sec. 3.3. In the overall training phase, We supervise the reconstruction model using mean squared error loss, LPIPS loss [44], and L1 depth loss as follows:

$$\mathcal{L}_{\text{recon}} = \mathcal{L}_{\text{mse}} + \lambda_1 \mathcal{L}_{\text{lpips}} + \lambda_2 \mathcal{L}_{\text{depth}}, \quad (3)$$

where λ_1 and λ_2 are the weights for each loss component. The depth supervision uses pseudo-labels produced by the off-the-shelf depth model [19].

3.2. Geometry-Aware Diffusion Refinement

Although the reconstruction model can effectively recover scene structures from multi-view images, it still struggles to produce high-quality and realistic results at free-viewpoint, especially for off-trajectory views. With the recent success of diffusion models in image generation [17, 30], we introduce a diffusion-based generation module to refine the feed-forward 3DGS renderings. Since the video diffusion model [3] has been extensively pre-trained on large-scale data, introducing additional parameters may degrade its generalization ability. Therefore, we keep our modification minimal to maintain compatibility and ensure stable generalization across diverse scenes.

To simplify the explanation, we describe the process using single image as examples. In practice, we employ a video diffusion model to ensure temporal consistency. For the geometry conditions C_{geo} rendered by the reconstruction model, we encode the geometry conditions into a condition latent representation $\mathbf{z}_c = \mathcal{E}_c(C_{\text{geo}})$ through a learnable condition encoder \mathcal{E}_c like [15]. During training, we encode the reference image I_r using a frozen image encoder \mathcal{E}_v to obtain the latent representation $\mathbf{z}_v = \mathcal{E}_v(I_r)$. Gaussian noise is added to the latent to obtain a noisy version [17] as follows:

$$\mathbf{z}_\tau = \alpha_\tau \mathbf{z}_v + \sigma_\tau \epsilon, \quad (4)$$

where $\epsilon \sim \mathcal{N}(0, 1)$ and τ is the diffusion timestep. The geometry condition latent \mathbf{z}_c is concatenated with the noise latent \mathbf{z}_τ along the channel dimension and fed into the diffusion model f_θ to predict the noise as follows:

$$\hat{\epsilon} = f_\theta(\mathbf{z}_\tau, \mathbf{z}_c). \quad (5)$$

The training objective [17] minimizes the mean squared error between the predicted and true noise as follows:

$$\mathcal{L}_{\text{gen}} = \mathbb{E}_{\tau, \mathbf{z}_v, \epsilon} [\|\epsilon - f_\theta(\mathbf{z}_\tau, \mathbf{z}_c)\|_2^2]. \quad (6)$$

This allows the diffusion model to learn geometry-aware refinement conditioned on the rendered scene structure.

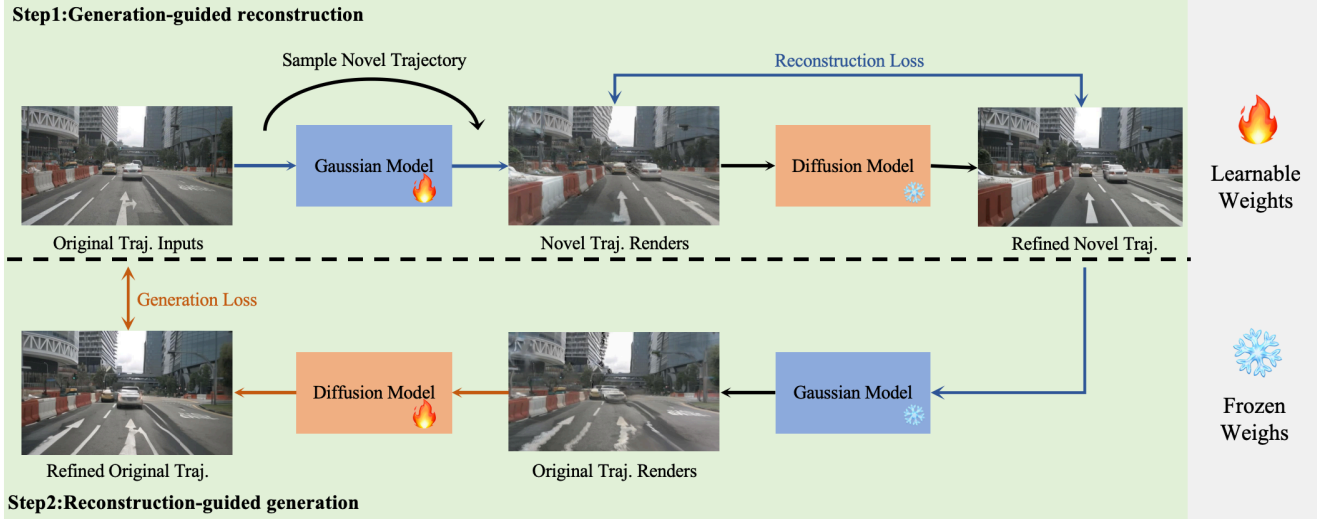


Figure 3. **Illustration of the Co-Training strategy.** FreeGen adopts a closed-loop co-training strategy between the Gaussian reconstruction model and the diffusion refinement model. Novel trajectories (Traj.) are sampled and rendered by the Gaussian model, then refined by the diffusion model to form pseudo-supervision. The refined results are fed back to the Gaussian model for reconstruction loss, while the diffusion model learns from generation loss on the original trajectory.

Table 2. **Quantitative comparison of free-viewpoint synthesis quality.** We compare FreeGen with existing methods under different trajectory shift settings. For fairness, the results of all baseline methods are taken from [15]. Auxiliary Information (Aux. Info.) indicates whether a method relies on additional data beyond images during training or inference, such as LiDAR point clouds or 3D bounding box annotations. All models are evaluated on six camera views.

Method	Aux. Info.	Shift $\pm 1m$		Shift $\pm 2m$		Shift $\pm 4m$	
		FID↓	FVD↓	FID↓	FVD↓	FID↓	FVD↓
PVG [6]	LiDAR & Box	48.15	246.74	60.44	356.23	84.50	501.16
EmerNeRF [41]	LiDAR & Box	37.57	171.47	52.03	294.55	76.11	497.85
StreetGaussian [40]	LiDAR & Box	32.12	153.45	43.24	256.91	67.44	429.98
OmniRe [8]	LiDAR & Box	31.48	152.01	43.31	254.52	67.36	428.20
FreeVS [36]	LiDAR & Box	51.26	431.99	62.04	497.37	77.14	556.14
DiST-4D [15]	LiDAR & Box	10.12	45.14	12.97	68.80	17.57	105.29
FreeGen (Ours)	None	9.49	32.83	11.34	44.98	14.44	70.75

Table 3. **Quantitative comparison on recorded views across different metrics.** We evaluate the performance on the original trajectory. **Image warping** refers to the geometric condition used by DiST-4D, while **Our Rec. model** is our reconstruction model.

Method	PSNR↑	SSIM↑	LPIPS↓
Image warping	18.14	0.58	0.42
Our Rec. model	20.40	0.62	0.36
DiST-4D [15]	23.85	0.74	0.29
FreeGen (Ours)	24.19	0.75	0.29

The generation model is also trained in two stages. In the first stage, we supervise the model with renderings and the corresponding ground-truth frames so that it learns to refine effectively under geometric conditions. In the sec-

ond stage, we introduce a closed-loop supervision scheme to improve generation quality at off-trajectory viewpoints. Details are provided in Sec. 3.3. The depth supervision follows the same protocol in Sec. 3.1.

3.3. Co-Training

Considering that both the reconstruction and generation models are trained with the single trajectory data, coverage of viewpoint variation is limited for free-viewpoint synthesis. Inspired by closed-loop training [15, 29] and noting that both models are learnable, we design a co-training scheme that lets the two models promote each other, as shown in Fig. 3. The procedure alternates two steps and freezes one model at a time to keep optimization stable.

Step 1: Generation-guided reconstruction. We randomly sample off-trajectory viewpoints and render them with the

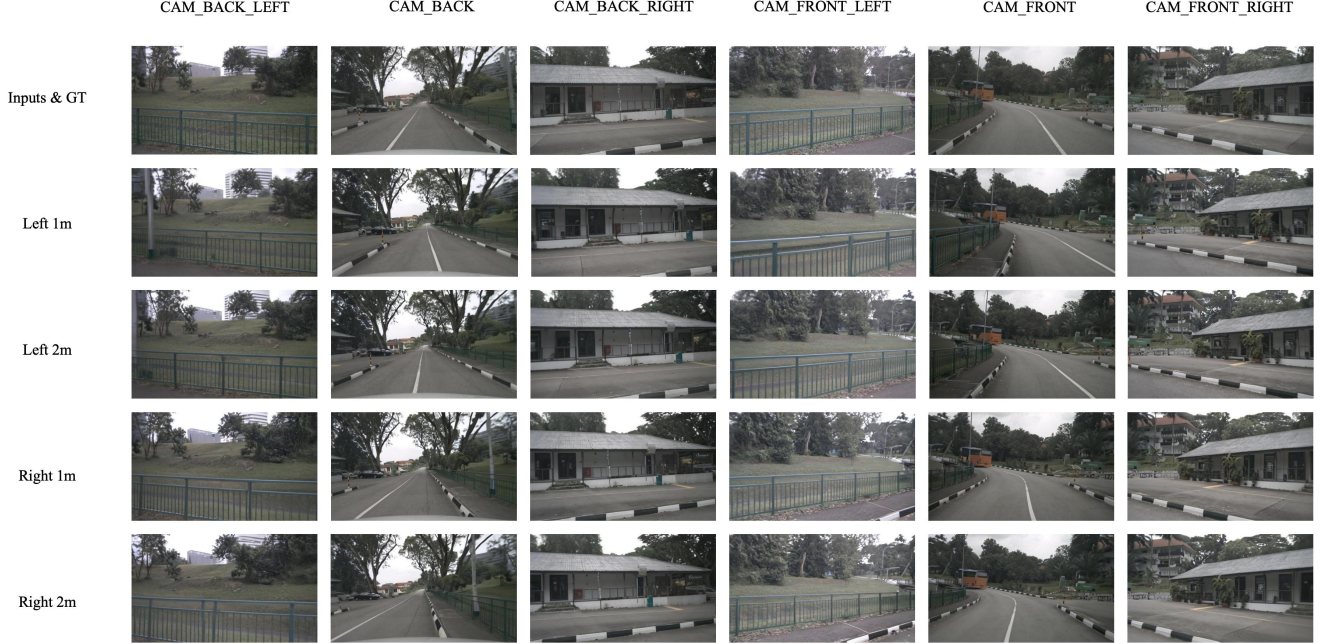


Figure 4. **Qualitative Results under Spatial Viewpoint Shifts.** We show generation results under lateral shifts of 1m and 2m to the left and right with six input views. Our method generates high-quality and detailed scenes while maintaining consistency across different viewpoints.

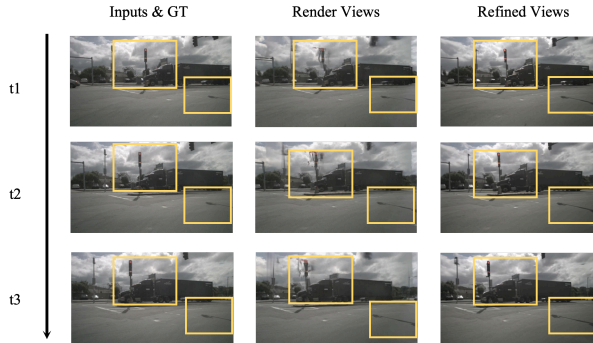


Figure 5. **Qualitative Results of Temporal Consistency.** We show three consecutive frames synthesized under a 1m lateral shift. For each timestamp, we present the ground-truth recorded image, the rendered views from the reconstruction model, and the refined results. The refined sequences remain temporally stable and preserve object geometry across time, highlighting the strong temporal consistency achieved by our method.

Gaussian model to obtain free-viewpoint images and their geometry conditions. The frozen diffusion model refines these off-trajectory renders and produces pseudo-labels. The Gaussian model is then updated on these pseudo-labels using the reconstruction losses defined in Sec. 3.1. This step transfers appearance priors to the reconstruction branch and improves its free-viewpoint rendering.

Step 2: Reconstruction-guided generation. Using the up-

dated Gaussian model, we take the off-trajectory renders and their refined results from Step 1 and render them back to the original trajectory viewpoints. The diffusion model refines these re-rendered views under geometric conditions and the outputs are supervised by the ground-truth frames with the generation losses in Sec. 3.2. This step strengthens geometry-aware refinement in the generation branch.

Through alternating Step 1 and Step 2 the reconstruction branch learns stronger off-trajectory geometry and the generation branch learns geometry-consistent appearance. The closed loop progressively aligns structural consistency and visual realism across free-viewpoints.

4. Experiments

4.1. Setup

Dataset. We conduct experiments on nuScenes [4]. Following prior work [15, 39], the 2 Hz keyframe annotations are interpolated to 12 Hz. We use the official split with 700 scenes for training and 150 scenes for validation.

Evaluation. For *off-trajectory evaluation*, we follow the protocols in [15, 36]. Specifically, we uniformly sample frames every two frames along the original recorded trajectory, and apply lateral camera shifts $\tau \in \{\pm 1\text{m}, \pm 2\text{m}, \pm 4\text{m}\}$ to each sampled frame. We synthesize RGB videos under the shifted viewpoints and compute Fréchet Inception Distance (FID) [31] and Fréchet Video Distance (FVD) [32] between the synthesized videos and

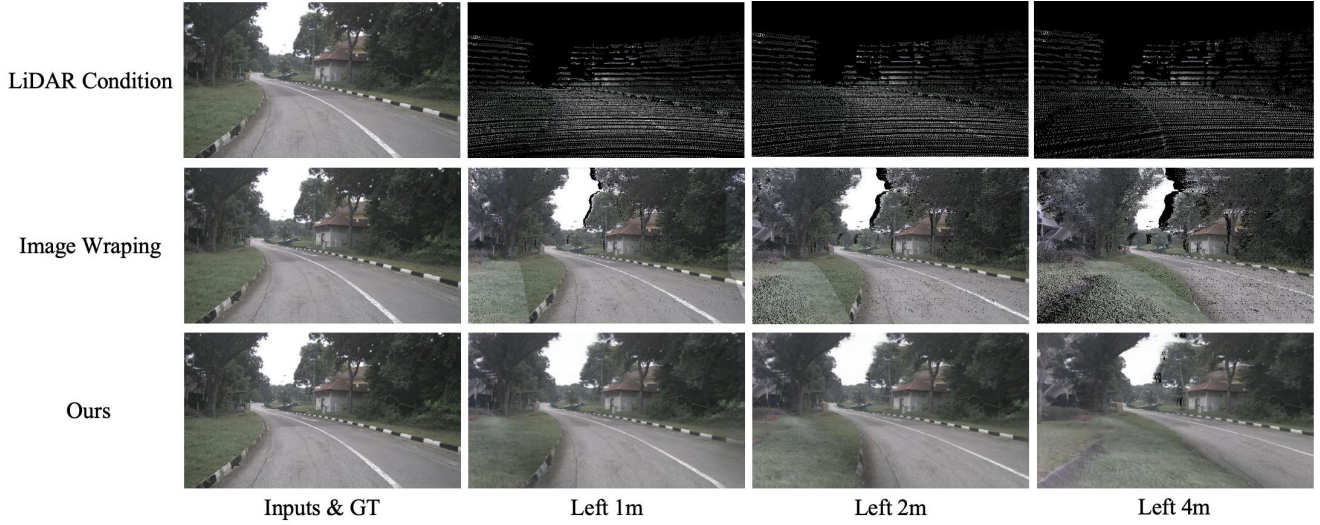


Figure 6. **Qualitative comparison of geometric conditions.** We construct target views with lateral shifts of 1 m, 2 m, and 4 m. For LiDAR-based conditions, we aggregate 10 consecutive frames and project the point clouds to the target view. For image warping, we use depth to warp the input images to the target camera. Our condition is obtained by rendering from the feed-forward reconstruction model.

Table 4. **Ablation study on the contribution of each module.** All metrics are evaluated under left 2m shift using six camera views. **Rec.** and **Gen.** indicate enabling the reconstruction and generation branches. **Opac.** denotes using the opacity maps as additional geometric condition. **Rec. CT** and **Gen. CT** indicate co-training the reconstruction branch and the generation branch respectively.

Settings	Rec.	Gen.	Opac.	Rec. CT	Gen. CT	FID-2m↓	FVD-2m↓
(a)	✓					23.25	246.73
(b)	✓	✓				15.49	60.53
(c)	✓	✓	✓			13.86	57.21
(d)	✓	✓	✓	✓		14.39	54.93
(e)	✓	✓	✓		✓	13.16	51.78
(f)	✓	✓	✓	✓	✓	13.05	50.92

the ground-truth videos rendered from the original trajectory. These metrics reflect appearance realism and temporal coherence under viewpoint extrapolation. For *on-trajectory evaluation*, we also sample frames every two frames, consistent with the training setup in [15], and generate views by shifting each sampled camera pose toward the next sampled viewpoint. We report peak signal-to-noise ratio (PSNR), structural similarity index (SSIM) [38], and perceptual similarity (LPIPS) [44] to assess reconstruction accuracy and perceptual fidelity along the original trajectory.

Implementation details. We use 768×432 resolution with video length of $T = 6$ for both training and inference, following [15]. The video diffusion model is initialized from Stable Video Diffusion (SVD) [3], following [15, 36]. λ_1 and λ_2 are set to 0.05 and 0.01 respectively, following [39]. All experiments run on two NVIDIA A100 GPUs. Please refer to the supplements for more implementation details.

4.2. Main Results

Off-trajectory Quantitative Evaluation. Table 2 reports results under three lateral shift settings. Classical reconstruction methods [6, 8, 40, 41] suffer from blur at off-trajectory viewpoints because no observations exist outside the input views, and they usually rely on LiDAR and boxes to supply depth and category cues for reconstruction. FreeVS [36] introduces extra geometry conditions by projecting LiDAR, but the point cloud is sparse and the aggregation requires boxes to separate dynamic from static objects, which limits performance. DiST-4D [15] uses image warping to provide geometry conditions and obtains noticeable gains, yet warping cannot faithfully represent full scene structure and the pipeline still depends on LiDAR and boxes with heavy preprocessing to recover depth. In contrast, our FreeGen achieves the best results at all shift levels. The improvements are especially large on FVD, indicating higher temporal coherence and realism under free-viewpoint changes. FreeGen uses only images and an off-the-shelf depth estimator to obtain depth in seconds, which is fast and easy to deploy at large scale.

On-trajectory Quantitative Evaluation. Table 3 presents the results on the original recorded trajectory. We first compare two types of geometric conditions on the recorded trajectory, namely the image warping conditions used in DiST-4D [15] and the geometry conditions rendered by our feed forward reconstruction model. As shown in Table 3, our reconstruction model provides more accurate geometry and produces images that are closer to the ground truth in both structure and perceptual quality. Table 3 also reports the results after generative refinement. FreeGen slightly im-

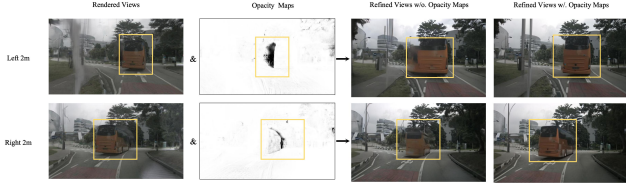


Figure 7. **Ablation on the opacity map.** We compare generation results with and without opacity guidance to assess its effect.

proves over DiST-4D [15] on PSNR and SSIM and matches its LPIPS. DiST-4D benefits from high quality depth maps that are constructed on the original trajectory using LiDAR and handcrafted processing. In contrast, our FreeGen only relies on an off-the-shelf depth model [19] yet still achieves comparable or better reconstruction quality on recorded trajectory views and stronger temporal and perceptual performance on off-trajectory evaluations. Moreover, when we compare the reconstructed views with the corresponding refined results, we observe that our co-training framework further enhances realism while still preserving high fidelity to the original scenes.

Qualitative Results. Fig. 4 shows qualitative results of FreeGen with six input views under lateral shifts of 1m and 2m to the left and right. Our method synthesizes sharp and detailed appearances while preserving scene geometry across viewpoints. Thin structures such as poles and lane markings remain intact and occlusion boundaries are stable. Cross-view consistency is maintained under all shifts, indicating that the geometry-aware refinement effectively guides high-quality free-viewpoint generation. Fig. 5 further presents qualitative results on temporal consistency. Across consecutive frames the refined views remain stable, without noticeable flickering or geometry drift.

4.3. Ablation Study

Main Ablation Studies. We conduct an ablation under a leftward shift of $-2m$ to validate each design choice. Table 4 reports the results for settings (a) to (f). (a) *Reconstruction only (Rec.)*. Novel views are rendered by the reconstruction model without generative refinement. This yields competitive FID due to faithful geometry but limited off-trajectory information and single-frame input lead to worse FVD. (b) *Generation (Gen.)*. Using the rendered color and depth to guide diffusion model improves both metrics, but the model lacks an explicit notion of reliable regions to refine. (c) *Opacity guidance (Opac.)*. Adding the opacity map provides reliability cues, which further improves performance. (d) *Co-training on reconstruction only (Rec.CT)*. We update the Gaussian branch with pseudo-labels refined by the generation model while keeping its trained on the single trajectory data. FVD improves due to better temporal stability while FID slightly drops, reflecting

Table 5. **Quantitative evaluation of different geometry conditions.** We compare the image warping condition used in DiST-4D with our geometric condition rendered by the feed-forward reconstruction model under different viewpoint shifts, using FID and FVD as metrics. OmniRe is included as a reference for the performance of the current best iterative reconstruction method.

Method	Shift $\pm 1m$		Shift $\pm 2m$		Shift $\pm 4m$	
	FID↓	FVD↓	FID↓	FVD↓	FID↓	FVD↓
OmniRe	31.48	152.01	43.31	254.52	67.36	428.20
Image wrapping	32.27	216.69	60.64	344.68	93.27	398.36
Our Rec. model	12.92	117.49	20.96	205.99	39.47	370.79

limited pseudo-label quality. (e) *Co-training on generation only (Gen.CT)*. We update the generation model with diverse off-trajectory renders. Both FID and FVD improve since the generation model observes a wider distribution of viewpoints. (f) *Co-training on both models*. Jointly updating reconstruction and generation models achieves the best results. The closed loop transfers appearance priors to the Gaussian model and supplies geometry-consistent supervision to the generation model, leading to the highest quality free-viewpoint driving scene synthesis.

Analysis of Geometry Conditions. We study how different geometry conditions affect generative refinement with both visualization and quantitative evaluation. Fig. 6 compares three types of conditions. FreeVS [36] projects LiDAR to the image plane. Even after aggregating 10 adjacent frames, the LiDAR condition remains sparse and is almost unusable for distant structures. DiST-4D [15] warps images to the target view and shows clearer layouts than LiDAR, yet it cannot represent full scene geometry and exhibits noticeable structural drift at larger viewpoint shifts. Our 3DGS-based condition captures scene structure and fine details in a few seconds and aligns well with the target view. Table 5 reports the metrics for LiDAR and reconstruction conditions. We exclude LiDAR projection from the table because the condition is too sparse to provide a fair comparison. Although our feed-forward reconstruction model uses only multi-view inputs from a single timestep at inference, the rendered geometry for new trajectories outperforms the current best iterative reconstruction pipeline. We attribute this to pretraining on large-scale data, which provides strong priors that improve predictions at off-trajectory viewpoints.

Analysis of Opacity Guidance. In Fig. 7, we visualize the effect of opacity guidance. The opacity map clearly highlights reliable and unreliable regions. With this guidance, the generative model can focus refinement on uncertain areas, which improves the overall quality of the results.

5. Conclusion

We have introduced FreeGen, a novel feed-forward framework for free-viewpoint driving scene synthesis from the single trajectory observations. Our approach effectively

addresses the critical challenge of balancing interpolation consistency and extrapolation realism. By co-training a reconstruction model with a generation model, FreeGen leverages the stable geometric guidance from reconstruction to ensure structural consistency, while harnessing the power of generative priors to enhance visual realism at unseen viewpoints. Extensive experiments demonstrate that FreeGen surpasses existing methods, enabling the efficient synthesis of high-fidelity and consistent driving scenes.

References

- [1] Jonathan T Barron, Ben Mildenhall, Dor Verbin, Pratul P Srinivasan, and Peter Hedman. Mip-nerf 360: Unbounded anti-aliased neural radiance fields. In *Proceedings of the IEEE/CVF conference on computer vision and pattern recognition*, pages 5470–5479, 2022. 2
- [2] Jonathan T Barron, Ben Mildenhall, Dor Verbin, Pratul P Srinivasan, and Peter Hedman. Zip-nerf: Anti-aliased grid-based neural radiance fields. In *Proceedings of the IEEE/CVF International Conference on Computer Vision*, pages 19697–19705, 2023. 2
- [3] Andreas Blattmann, Tim Dockhorn, Sumith Kulal, Daniel Mendelevitch, Maciej Kilian, Dominik Lorenz, Yam Levi, Zion English, Vikram Voleti, Adam Letts, et al. Stable video diffusion: Scaling latent video diffusion models to large datasets. *arXiv preprint arXiv:2311.15127*, 2023. 1, 2, 3, 4, 7
- [4] Holger Caesar, Varun Bankiti, Alex H Lang, Sourabh Vora, Venice Erin Liong, Qiang Xu, Anush Krishnan, Yu Pan, Giancarlo Baldan, and Oscar Beijbom. nuscenes: A multi-modal dataset for autonomous driving. In *Proceedings of the IEEE/CVF conference on computer vision and pattern recognition*, pages 11621–11631, 2020. 1, 6
- [5] David Charatan, Sizhe Lester Li, Andrea Tagliasacchi, and Vincent Sitzmann. pixelsplat: 3d gaussian splats from image pairs for scalable generalizable 3d reconstruction. In *Proceedings of the IEEE/CVF conference on computer vision and pattern recognition*, pages 19457–19467, 2024. 3, 4
- [6] Yurui Chen, Chun Gu, Junzhe Jiang, Xiatian Zhu, and Li Zhang. Periodic vibration gaussian: Dynamic urban scene reconstruction and real-time rendering. *arXiv preprint arXiv:2311.18561*, 2023. 1, 5, 7
- [7] Yuedong Chen, Haofei Xu, Chuanxia Zheng, Bohan Zhuang, Marc Pollefeys, Andreas Geiger, Tat-Jen Cham, and Jianfei Cai. Mvsplat: Efficient 3d gaussian splatting from sparse multi-view images. In *European Conference on Computer Vision*, pages 370–386. Springer, 2024. 3, 4
- [8] Ziyu Chen, Jiawei Yang, Jiahui Huang, Riccardo de Lutio, Janick Martinez Esturo, Boris Ivanovic, Or Litany, Zan Gojcic, Sanja Fidler, Marco Pavone, et al. Omnire: Omni urban scene reconstruction. *arXiv preprint arXiv:2408.16760*, 2024. 1, 5, 7
- [9] Prafulla Dhariwal and Alexander Nichol. Diffusion models beat gans on image synthesis. *Advances in neural information processing systems*, 34:8780–8794, 2021. 3
- [10] Lue Fan, Hao Zhang, Qitai Wang, Hongsheng Li, and Zhaoxiang Zhang. Freesim: Toward free-viewpoint camera simulation in driving scenes. In *Proceedings of the Computer Vision and Pattern Recognition Conference*, pages 12004–12014, 2025. 1, 2
- [11] Ruiyuan Gao, Kai Chen, Enze Xie, Lanqing Hong, Zhenguo Li, Dit-Yan Yeung, and Qiang Xu. Magicdrive: Street view generation with diverse 3d geometry control. *arXiv preprint arXiv:2310.02601*, 2023. 1, 3
- [12] Ruiyuan Gao, Kai Chen, Bo Xiao, Lanqing Hong, Zhenguo Li, and Qiang Xu. Magicdrive-v2: High-resolution long video generation for autonomous driving with adaptive control. In *Proceedings of the IEEE/CVF International Conference on Computer Vision*, pages 28135–28144, 2025. 1
- [13] Shenyuan Gao, Jiazhi Yang, Li Chen, Kashyap Chitta, Yihang Qiu, Andreas Geiger, Jun Zhang, and Hongyang Li. Vista: A generalizable driving world model with high fidelity and versatile controllability. *Advances in Neural Information Processing Systems*, 37:91560–91596, 2024. 1, 3
- [14] Andreas Geiger, Philip Lenz, and Raquel Urtasun. Are we ready for autonomous driving? the kitti vision benchmark suite. In *2012 IEEE conference on computer vision and pattern recognition*, pages 3354–3361. IEEE, 2012. 1
- [15] Jiazhe Guo, Yikang Ding, Xiwu Chen, Shuo Chen, Bohan Li, Yingshuang Zou, Xiaoyang Lyu, Feiyang Tan, Xiaojuan Qi, Zhiheng Li, et al. Dist-4d: Disentangled spatiotemporal diffusion with metric depth for 4d driving scene generation. *arXiv preprint arXiv:2503.15208*, 2025. 1, 2, 3, 4, 5, 6, 7, 8
- [16] Jonathan Ho and Tim Salimans. Classifier-free diffusion guidance. *arXiv preprint arXiv:2207.12598*, 2022. 3
- [17] Jonathan Ho, Ajay Jain, and Pieter Abbeel. Denoising diffusion probabilistic models. *Advances in neural information processing systems*, 33:6840–6851, 2020. 4
- [18] Jonathan Ho, Tim Salimans, Alexey Gritsenko, William Chan, Mohammad Norouzi, and David J Fleet. Video diffusion models. *Advances in neural information processing systems*, 35:8633–8646, 2022. 3
- [19] Mu Hu, Wei Yin, Chi Zhang, Zhipeng Cai, Xiaoxiao Long, Hao Chen, Kaixuan Wang, Gang Yu, Chunhua Shen, and Shaojie Shen. Metric3d v2: A versatile monocular geometric foundation model for zero-shot metric depth and surface normal estimation. *IEEE Transactions on Pattern Analysis and Machine Intelligence*, 2024. 4, 8
- [20] Shengchao Hu, Li Chen, Penghao Wu, Hongyang Li, Junchi Yan, and Dacheng Tao. St-p3: End-to-end vision-based autonomous driving via spatial-temporal feature learning. In *European Conference on Computer Vision*, pages 533–549. Springer, 2022. 1
- [21] Yihan Hu, Jiazhi Yang, Li Chen, Keyu Li, Chonghao Sima, Xizhou Zhu, Siqi Chai, Senyao Du, Tianwei Lin, Wenhai Wang, et al. Planning-oriented autonomous driving. In *Proceedings of the IEEE/CVF conference on computer vision and pattern recognition*, pages 17853–17862, 2023. 1
- [22] Yuanhui Huang, Wenzhao Zheng, Yunpeng Zhang, Jie Zhou, and Jiwen Lu. Tri-perspective view for vision-based 3d semantic occupancy prediction. In *Proceedings of the IEEE/CVF conference on computer vision and pattern recognition*, pages 9223–9232, 2023. 4

- [23] Bo Jiang, Shaoyu Chen, Qing Xu, Bencheng Liao, Jiajie Chen, Helong Zhou, Qian Zhang, Wenyu Liu, Chang Huang, and Xinggang Wang. Vad: Vectorized scene representation for efficient autonomous driving. In *Proceedings of the IEEE/CVF International Conference on Computer Vision*, pages 8340–8350, 2023. 1
- [24] Bernhard Kerbl, Georgios Kopanas, Thomas Leimkühler, and George Drettakis. 3d gaussian splatting for real-time radiance field rendering. *ACM Trans. Graph.*, 42(4):139–1, 2023. 1, 2, 4
- [25] Zhiqi Li, Wenhao Wang, Hongyang Li, Enze Xie, Chonghao Sima, Tong Lu, Qiao Yu, and Jifeng Dai. Bevformer: learning bird’s-eye-view representation from lidar-camera via spatiotemporal transformers. *IEEE Transactions on Pattern Analysis and Machine Intelligence*, 2024. 4
- [26] Ben Mildenhall, Pratul P Srinivasan, Matthew Tancik, Jonathan T Barron, Ravi Ramamoorthi, and Ren Ng. Nerf: Representing scenes as neural radiance fields for view synthesis. *Communications of the ACM*, 65(1):99–106, 2021. 2
- [27] Thomas Müller, Alex Evans, Christoph Schied, and Alexander Keller. Instant neural graphics primitives with a multiresolution hash encoding. *ACM transactions on graphics (TOG)*, 41(4):1–15, 2022. 2
- [28] Chaojun Ni, Guosheng Zhao, Xiaofeng Wang, Zheng Zhu, Wenkang Qin, Guan Huang, Chen Liu, Yuyin Chen, Yida Wang, Xueyang Zhang, et al. Recondreamer: Crafting world models for driving scene reconstruction via online restoration. In *Proceedings of the Computer Vision and Pattern Recognition Conference*, pages 1559–1569, 2025. 1, 2
- [29] Xuanchi Ren, Tianchang Shen, Jiahui Huang, Huan Ling, Yifan Lu, Merlin Nimier-David, Thomas Müller, Alexander Keller, Sanja Fidler, and Jun Gao. Gen3c: 3d-informed world-consistent video generation with precise camera control. In *Proceedings of the Computer Vision and Pattern Recognition Conference*, pages 6121–6132, 2025. 5
- [30] Robin Rombach, Andreas Blattmann, Dominik Lorenz, Patrick Esser, and Björn Ommer. High-resolution image synthesis with latent diffusion models. In *Proceedings of the IEEE/CVF conference on computer vision and pattern recognition*, pages 10684–10695, 2022. 3, 4
- [31] Maximilian Seitzer. pytorch-fid: FID Score for PyTorch. <https://github.com/mseitzer/pytorch-fid>, 2020. Version 0.3.0. 6
- [32] Ivan Skorokhodov, Sergey Tulyakov, and Mohamed Elhoseiny. Stylegan-v: A continuous video generator with the price, image quality and perks of stylegan2, 2021. 6
- [33] Jiaming Song, Chenlin Meng, and Stefano Ermon. Denoising diffusion implicit models. *arXiv preprint arXiv:2010.02502*, 2020. 3
- [34] Pei Sun, Henrik Kretschmar, Xerxes Dotiwalla, Aurelien Chouard, Vijaysai Patnaik, Paul Tsui, James Guo, Yin Zhou, Yuning Chai, Benjamin Caine, et al. Scalability in perception for autonomous driving: Waymo open dataset. In *Proceedings of the IEEE/CVF conference on computer vision and pattern recognition*, pages 2446–2454, 2020. 1
- [35] Qijian Tian, Xin Tan, Yuan Xie, and Lizhuang Ma. Drivingforward: Feed-forward 3d gaussian splatting for driving scene reconstruction from flexible surround-view input. In *Proceedings of the AAAI Conference on Artificial Intelligence*, pages 7374–7382, 2025. 1, 3, 4
- [36] Qitai Wang, Lue Fan, Yuqi Wang, Yuntao Chen, and Zhaoxiang Zhang. Freevs: Generative view synthesis on free driving trajectory. *arXiv preprint arXiv:2410.18079*, 2024. 1, 2, 3, 5, 6, 7, 8
- [37] Xiaofeng Wang, Zheng Zhu, Guan Huang, Xinze Chen, Jia-gang Zhu, and Jiwen Lu. Drivedreamer: Towards real-world-drive world models for autonomous driving. In *European conference on computer vision*, pages 55–72. Springer, 2024. 1, 3
- [38] Zhou Wang, Alan C Bovik, Hamid R Sheikh, and Eero P Simoncelli. Image quality assessment: from error visibility to structural similarity. *IEEE transactions on image processing*, 13(4):600–612, 2004. 7
- [39] Dongxu Wei, Zhiqi Li, and Peidong Liu. Omni-scene: Omni-gaussian representation for ego-centric sparse-view scene reconstruction. In *Proceedings of the Computer Vision and Pattern Recognition Conference*, pages 22317–22327, 2025. 1, 2, 3, 4, 6, 7
- [40] Yunzhi Yan, Haotong Lin, Chenxu Zhou, Weijie Wang, Haiyang Sun, Kun Zhan, Xianpeng Lang, Xiaowei Zhou, and Sida Peng. Street gaussians: Modeling dynamic urban scenes with gaussian splatting. In *European Conference on Computer Vision*, pages 156–173. Springer, 2024. 1, 2, 3, 5, 7
- [41] Jiawei Yang, Boris Ivanovic, Or Litany, Xinshuo Weng, Seung Wook Kim, Boyi Li, Tong Che, Danfei Xu, Sanja Fidler, Marco Pavone, et al. Emernerf: Emergent spatial-temporal scene decomposition via self-supervision. *arXiv preprint arXiv:2311.02077*, 2023. 1, 5, 7
- [42] Ze Yang, Yun Chen, Jingkan Wang, Sivabalan Manivasagam, Wei-Chiu Ma, Anqi Joyce Yang, and Raquel Urtasun. Unisim: A neural closed-loop sensor simulator. In *Proceedings of the IEEE/CVF Conference on Computer Vision and Pattern Recognition*, pages 1389–1399, 2023. 1
- [43] Zeyu Yang, Zijie Pan, Yuankun Yang, Xiatian Zhu, and Li Zhang. Driving scene synthesis on free-form trajectories with generative prior. *arXiv preprint arXiv:2412.01717*, 2024. 1, 2, 3
- [44] Richard Zhang, Phillip Isola, Alexei A Efros, Eli Shechtman, and Oliver Wang. The unreasonable effectiveness of deep features as a perceptual metric. In *Proceedings of the IEEE conference on computer vision and pattern recognition*, pages 586–595, 2018. 4, 7
- [45] Guosheng Zhao, Chaojun Ni, Xiaofeng Wang, Zheng Zhu, Xueyang Zhang, Yida Wang, Guan Huang, Xinze Chen, Boyuan Wang, Youyi Zhang, et al. Drivedreamer4d: World models are effective data machines for 4d driving scene representation. In *Proceedings of the Computer Vision and Pattern Recognition Conference*, pages 12015–12026, 2025. 1, 2, 3